Geoscience Frontiers 7 (2016) 287–294

HOSTED BY

Contents lists available at ScienceDirect

China University of Geosciences (Beijing)

Geoscience Frontiers

journal homepage: www.elsevier.com/locate/gsf

Research paper

GIS-based analysis of fault patterns in urban areas: A case study of Irkutsk city, Russia

R.M. Lobatskaya*, I.P. Strelchenko

Irkutsk Research Technological University, Irkutsk, Russia

ARTICLE INFO

Article history:
Received 2 April 2014
Received in revised form
30 June 2015
Accepted 18 July 2015
Available online 7 August 2015

Keywords:
GIS
3D modeling
Fault pattern
Faults
Blocks
Ground stability

ABSTRACT

The capabilities of GIS in modeling fault patterns are explored for Irkutsk city in East Siberia with implications for ground stability. The neotectonic structure of the area is visualized in three dimension (3D) taking into account fault dips, using the ArcGIS, GlobalMapper and Paradigm Geophysical packages. The study area is divided into blocks of different size classes according to the length-based ranks of the bounding faults, which are of five classes distinguished with the equal interval method. The blocks show different deformation patterns, with different densities and strikes of crossing and bounding faults. The data are statistically processed using GIS to estimate the deformation degrees of blocks in arbitrary units per square kilometer using the attributes of rank and crossing/bounding position of faults and the size of blocks. The deformation degrees are then compared with available estimates of ground stability measured as a score of points corresponding to destabilizing factors. Although the comparison generally confirms some linkage between the deformation degree of blocks and their ground stability, the correlation is intricate and ambiguous. In order to enhance the advantages of GIS in building and analyzing 3D models of fault patterns for estimating ground stability and mitigating geological hazards, it is expected in the future to proceed from the reported initial step of visualization to more advanced analysis.

1. Introduction

Faults control many geological processes (Sherman, 1977; Lobatskaya, 1987; Sibson, 1987, 2001, 2006; Koff and Lobatskaya, 1991; Logatchev, 1991; Lobatskaya and Koff, 1997; Gonzalez et al., 2006; Archegov, 2012; Healy et al., 2012; Büttner et al., 2013; Carlos et al., 2014). Permeable faulted crust may be a favorable environment in terms of metallogeny but may pose hazard problems to densely populated and industrial urban territories. To mitigate the stability risks for building and engineering structures in cities, fault patterns can be mapped using advanced geoinformation technologies.

Unlike pristine lands, urban areas are subject to joint action of natural and man-made processes. Human impacts can affect the original site conditions, and especially, the natural ground stability which is responsible for the capacity of foundations to bear natural and cultural static and dynamic loads for the design life of structures (Lobatskaya, 1997, 2001, 2008; Lobatskaya and Koff, 1998; Makarov, 2007). In this geotechnical context, it is important to monitor near-surface ground stability at depths from tens to hundreds of meters, depending on the designed loads.

Ground stability is controlled by the lithology and physics of soils, which may change as a result of external natural and/or industrial geomechanical effects. Due regard for integrated lithological and mechanic parameters is indispensable for estimating the current state of the ground and predicting its future behavior under increasing anthropogenic impacts and natural hazards (Lobatskaya, 1997, 2001, 2008; Lobatskaya and Kotlobaeva, 2001).

The strength and water content of soils are controlled naturally by terrain ruggedness, faulting, erosion, etc. As shown by special analysis of twenty geological, geotechnical, geophysical, and mechanic parameters, they have different contributions to the total ground stability, but the greatest risks are associated with faults (Lobatskaya and Koff, 1998; Lobatskaya, 2008).

Being active geological, geomorphic, and environmental agents, faults can interfere with technology-related processes. Natural and technological hazards in faulted areas cause 90% more emergency than in the undeformed ground (Lobatskaya and Koff, 1998), and can have disastrous consequences. Faults provoke seismicity,

* Corresponding author.
E-mail address: lobatskaya@gmail.com (R.M. Lobatskaya).
Peer-review under responsibility of China University of Geosciences (Beijing).

http://dx.doi.org/10.1016/j.gsf.2015.07.004

accelerate natural erosion, and make human impacts on the environment at least tens of times greater. On the other hand, the interference of man can trigger or speed up faulting and induce seismicity even in stable areas, as it may happen, for instance, during large waterwork installations (Lobatskaya, 2001, 2008).

Although posing great risks to ground stability, faults in urban territories remain insufficiently studied, and the appropriate mapping methods are poorly developed. The reasons may be the complexity of fault parameters and their correlations, as well as problems with mapping fault patterns in technogenic landscapes. We are using GIS and advance data processing techniques, adapted and updated to correlate the parameters of faults with ground stability and its controls. The aim is to demonstrate the effectiveness of GIS for neotectonic modeling with regard to dips of faults.

The issues concerning the role of faults in urban territories are diverse and may be a subject of long multi-stage research. This study is limited to GIS-based 2D and 3D visualization of the fault pattern within Irkutsk city and checking the applicability of the approach to further ground stability research.

More specifically, the objectives are: (i) choice of study area; (ii) modeling fault pattern in 2D; (iii) building a 3D solid model of faults and blocks, with regard to fault dips; (iv) analysis of the 3D solid model and its application to building a generalized map of blocks; (v) predicting ground stability in the city on the basis of modeling results.

2. Data and methods

The study was carried out in the urban area of Irkutsk city, which is a well documented territory located within the Lake Baikal region of active faulting and seismicity. Numerous faults of different orientations in the area are of interest for 2D and 3D visualization while ground stability issues are urgent for the densely populated industrial city.

Modeling was based on (i) earlier and new field data collected from trenches, boreholes, and natural outcrops (Koff et al., 1996; Lobatskaya, 1997); (ii) structural measurements along and across inferred faults; (iii) data of common mid-point (CMP) reflection profiling (Lobatskaya, 2001; Lobatskaya and Kotlobaeva, 2001); (iv) satellite imagery (Lobatskaya, 2008).

GIS-based 2D and 3D neotectonic modeling was performed using the ArcGIS, GlobalMapper and Paradigm Geophysical packages. The field data were processed to image the fault pattern in a 1:25,000 digital map for the territory of Irkutsk and its suburbs, this scale being sufficient for GIS applications to ground stability analysis in urban territories. GIS mapping was preceded by creating a database (Thayer et al., 2004; ArcGIS Desktop, 2010), which included layers of faults and rivers.

Faults were laid over the topographic basemap using the ESRI desktop ArcMap10 software (Breunig et al., 1999, 2000; Gardoll et al., 2000). The topographic basemap was created by ArcGIS digitizing of paper maps because the Irkutsk territory lacks a digital elevation model (DEM), which would enable precise location of faults and substitute for deciphering remote sensing data.

Digital 3D modeling of faults was made with the GeoDepth Paradigm Geophysical software used by petroleum and geophysical service companies as a seismic imaging tool. The input data included terrain gradients provided by the SRTM (Shuttle Radar Topographic Mission) GlobalMapper digital elevation model and fault depths.

The workflows of 2D and 3D modeling are summarized in separate charts (Tables 1 and 2).

3. Mapping fault pattern (2D visualization)

After the database had been created and the paper maps were digitized, the basic linear model of faults, or a fault overlay, was obtained by populating the basemap with attributes of faults and blocks (Fig. 1). The selected parameters included size ranks of faults and blocks, fault lengths, fault orientations within blocks and across the area, fault density in blocks of different sizes, geometry of faults and blocks, etc (Table 1).

Table 1
Workflow chart for 2D modeling of faults (ArcGIS).

1	Load and reference topographic basemap (raster)
2	Create a database consisting of faults of different sizes and geometries (linear objects), blocks of different sizes (polygons), and drainage network (linear and polygon layers)
3	Map faults laid over raster basemap according to field data
4	Populate attribute table of linear layers with fault names, lengths, geometries (normal, reverse, or uncertain), dips, and ranks, and with river names
5	Group faults into five ranks on the basis of length (Symbology tab in Layer properties window)
6	Choose color scale and thickness for faults of different ranks (Symbology tab in Layer properties window)
7	Lay out fault map, create legend and export map in any raster format

Faults were detected and ranked using the classification of quantitative data. The spatial objects were grouped according to attribute values using the method of equal intervals dividing the range of attribute values into equal-sized subranges. This method was chosen among different ways of grouping (Cassard et al., 2004; Cheremisina and Nikitin, 2006; ArcGIS Desktop, 2010) as most appropriate for our purposes and conditions.

In ranking faults and blocks, the main focus was placed on fault length as the basic criterion (Sherman, 1977). The length of a fault, as any linear spatial object, is a system parameter computed automatically from spatially tied input data. To add values to the respective column of the attribute table, it is enough to choose the metric units and apply the Geometry option (ArcGIS Desktop, 2010).

The faults in the Irkutsk territory, ranked according to their lengths, form a series of a five-grade scale: $<$6.7 km (I), 6.8–12.4 km (II), 12.5–18.1 km (III), 18.2–23.8 km (IV), and $>$23.9 km (V). Statistically, faults of rank I are the most typical while longer or shorter faults are quite few in the area. The faults of rank I strike mainly to the northwest at 315°–320° or to the northeast, with a broad range of azimuths: 10°–15°, 20°, 40°, 50°–60°.

There are two regional-scale faults longer than 23.9 km (rank V): the N–S Angara and W–E Irkut-Ushakovka faults. The largest Angara fault is clearly expressed geomorphically coinciding with the tectonic valley of the Angara River in the present structural framework. About 2.5 km northwest of the Irkut River, it forks into larger and smaller arms that run along the right and left Angara banks, respectively. The Irkut-Ushakovka, another large fault, is younger than the Anagra fault and crosscuts and displaces the latter near the Irkut mouth. It has a right-lateral strike-slip geometry delineated by the bend of the Anagara between the mouths of its two tributaries: the Irkut and the Ushakovka.

As a result, 2D visualization of fault groups with lines of different thicknesses and colors has highlighted fault-bounded blocks. The obtained map (Fig. 1) constitutes the basis for 3D tectonic modeling of the city territory; the 3D solid model of faults and blocks, in turn, can be used for further analysis (Bilibin et al., 2007; Archegov, 2012).

4. Building a 3D solid model of faults and blocks with regard to fault dips

Creating 3D solid models is a broadly used tool for the study of fault patterns for different purposes (Krasnoramenskaya, 2008;

Table 2
Workflow chart for building a 3D solid model of faults and blocks (GlobalMapper, Paradigm Geophysical).

1		Create vector layer of faults (Table 1)
2		Convert vector layer of faults to *.txt or *.gen format (run ArcGIS: ArcMap, ArcView)
3		Obtain DEM in required coordinates (run GlobalMapper)
4		Import data to GeoDepth system (run Paradigm Geophysical)
5		Grid imported data (DEM and vector layer of faults) (run IMap)
6	Cycle, for each fault	Search and fix fault intersections with vertical grid lines and pass to Section module
7	Cycle, for each fault	Determine fault dips (see Table of layer attributes in ArcGIS) and calculate shifts of picks (BC in Fig. 3) as BC = AC/tgα where AC and ∠α are, respectively, depth and dip of fault
8	Cycle, for each fault	Pick faults with regard to shift, use paint tool with side guides (in Section module)
9	Cycle, for each fault	Merge picks into T-surfaces (run Create T-surface from picks in Canvas)
10		Transform DEM into T-surfaces (run Create T-surface from grid in Canvas)
11		Create Dominance table of faults (select Model Building→Dominance Table options in Canvas)
12		Repair T-surfaces of faults and DEM according to Dominance table (select Model Building→Repair T-surfaces options in Canvas)
13		Build 3D model (select Model Building→Create solid model option in Canvas)
14		Choose color scale for visualizing blocks of different ranks (in GeoDepth Surface Table)

Lobatskaya and Krasnoramenskaya, 2010; Nengxiong et al., 2011). When being imaged in the depth dimension, faults are commonly assumed to be normally dipping planes, but in this approach some important features may remain overlooked. Instead, it appears more reasonable to take into account the dip of faults, which has bearing on deformation. The deformation division is made into depth intervals distinguished on the basis of fault ranks in the 2D model (Lobatskaya and Krasnoramenskaya, 2010). Note that the depthward geometries and deformation degrees of the blocks are neglected at this stage.

Fault depths, put into the model together with SRTM terrain gradients, were assumed as intervals corresponding to brittle, quasi-plastic, plastic, and viscous flow deformation responsible for rupture and/or slip. The depths of faults (H) were related to their lengths (L) according to the empirical relationships indicating that the depth increment decreases proportionally to the length. The relationship was first suggested by Sherman and Lobatskaya (1972) to be $H/L \approx 1$ in 6–20 km long faults and then updated by Sankov (1989) for other fault lengths.

Special attention in 3D modeling was given to faults of ranks III, IV, and V which define the deformation pattern in the uppermost crust relevant to estimating the stability of soils (shallowest fault blocks); faults of ranks I and II were taken into account as well for appropriate ranking of blocks. The fault dips were assumed to be 60° proceeding from the dip range between 50° and 70° measured in the field.

The 3D neotectonic solid model was built on the basis of maps and linear faults transformed into surfaces and repaired (adjusted to one another to make them consistent) (Trufanova and Kazantseva, 2005; Trufanova et al., 2008; Strelchenko, 2013), using simultaneously three GeoDepth modules that process geodata laterally (IMap) and in depth (Section), and build 3D solid models (Canvas).

Canvas converts maps as the GlobalMapper DEMs into T-surface models as 2D triangulation surfaces created in 3D Canvas. The procedure of creating T-surfaces is launched by the respective algorithm and does not require special efforts. Most of work consists in selecting fault lines, bringing them together into surfaces, and repairing the surfaces.

The fault picks are projections of dipping faults in depth (Fig. 2) obtained simultaneously in the IMap and Section modules (Paradigm Geophysical, 2007). IMap performs gridding of the GlobalMapper DEM with a vector fault overlay on it. The vertical and horizontal grid spacing values are specified by the user depending on the desired selection resolution. The values 1 and 100 are assigned, respectively, to the leftmost vertical and lowermost horizontal (1) and to the rightmost vertical and the top horizontal (100) lines. Selection occurs at the points in IMap where the fault crosses the vertical grid. Faults are approximated by several intercepts with their number corresponding to the number of intersections with the grid. The resulting chosen faults and their formalization are presented in the Section module.

Faults are chosen one by one, the procedure being as follows. A fault is first traced horizontally in IMap and then becomes imaged in a vertical plane (already in the Section module) at the points where it crosses a vertical grid line (Fig. 2). Therefore, the selection of faults starts at the intersection of inline (X coordinate) and crossline (Y coordinate) values in IMap corresponding to the respective terrain profile. The program is not meant to deal with angles, the shift of selected faults is estimated relative to the vertical as a function of fault depths and dips, proceeding from the laws of right triangles and alternate angles (the leg BC of the right triangle in Fig. 2): $BC = H/\tan\alpha$, where BC is the shift, H is the depth reached by the fault (AC), and α is the tangent of the fault dip. Further work on creating and repairing the fault T-surfaces is run in Canvas. For creating T-surfaces, it is enough to carefully select parameters for the respective algorithm, while the program itself suggests the ways and succession of linking the upper and lower points of picks. For this study, the Gridding parameter is selected.

The intersecting surfaces are repaired (Fig. 3), using a Dominance Table created by rating each fault in terms of its dominance over other faults according to length and depth. Physically the repairing procedure consists in imaging pairs of intersecting faults in a T-shaped way by means of trimming the inferior fault in the pair according to the dominance table.

The intersections may be either systematic or real (Fig. 4). Systematic intersections naturally arise in surface modeling with fault picks. In this case, the priority is given to deeper and longer faults, and the Canvas algorithms (Extrapolation Repair or Trim) automatically trim the faults to provide their tight fit to the priority one. In the case of real intersections of several faults, the priority is given to larger faults as well, but the surfaces of inferior faults are divided

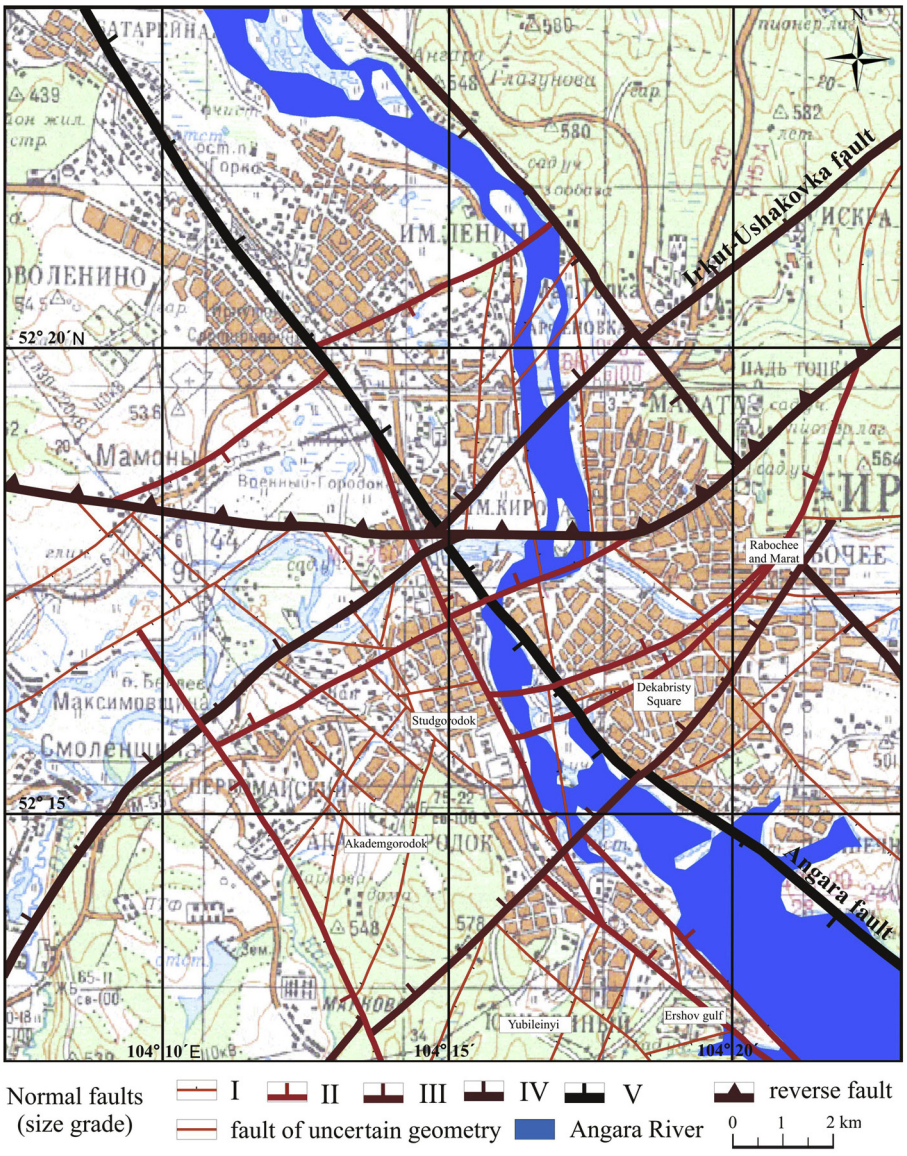

Figure 1. Map of faults of Irkutsk city.

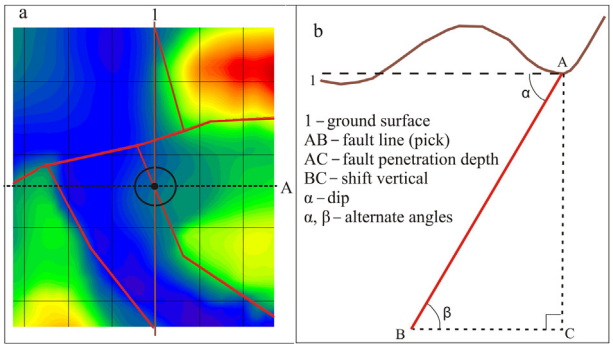

Figure 2. Sketch of fault picking. The terrain profile corresponds to the vertical plane and A to the horizontal plane (map). (a) Picking in map view; (b) picking in section view.

into independent T-surfaces at the intersections. For this, the picks are brought together into two (instead of one) surfaces which overlap at intersections with the dominant fault. This actually leads to systematic intersections correctable as above, and the main fault surface thus remains solid. The method is well applicable to dipping faults.

Accordingly, the dominance table was created in two ways for faults of different orientations, in order to image more faithfully the complex tectonic framework of the city area. One way was to select the dominant fault as the one which is long and is neither offset nor confined by other faults. In our case it was the Irkut-Ushakovka right-lateral strike-slip fault. The other way was to divide large faults (such as the Angara one) into independent T-surfaces at points where the mapped fault line was offset by another crossing fault.

Finally, the algorithm of 3D solid model building has yielded a cube consisting of neotectonic blocks of different sizes (Fig. 5). Although the model cannot be used for calculations yet without being converted to a GIS format, it provides visualization required

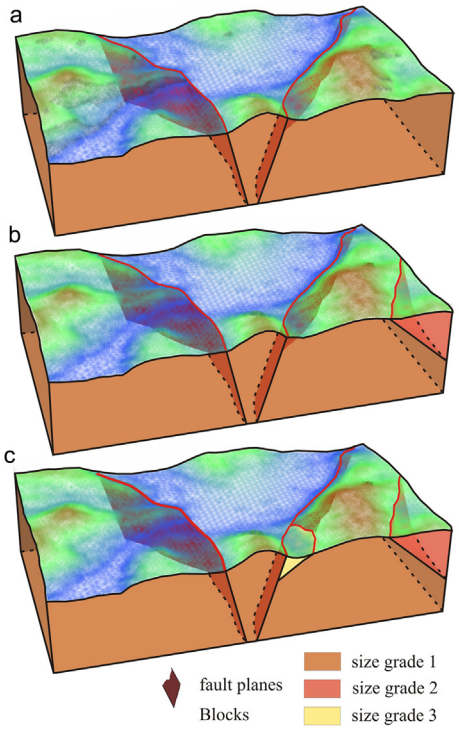

Figure 3. Tentative 3D solid model. (a, b, c) are steps of including blocks of different size ranks.

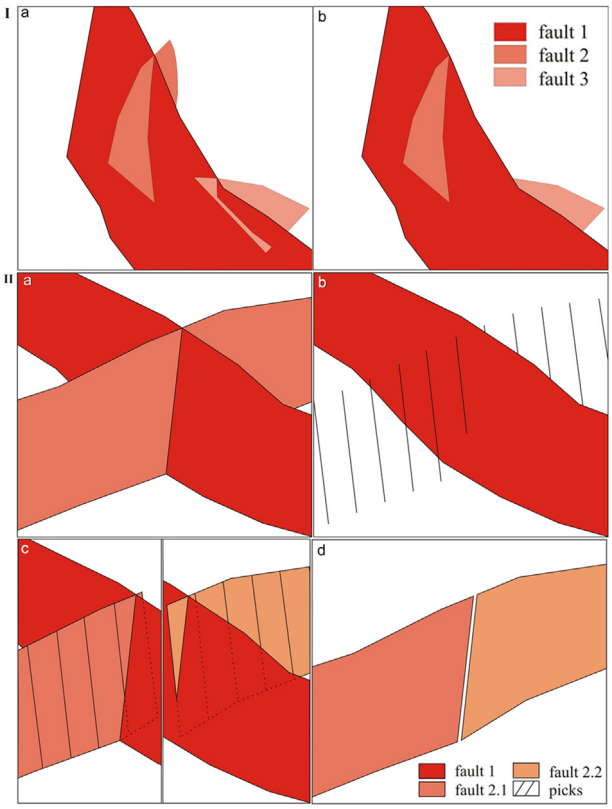

Figure 4. Fault intersections and repairing. I–systematic intersection: (a) before repairing, (b) after repairing; II–real intersection: (a) before repairing, (b, c) two ways of repairing: choice of priority fault (solid) and trimming (b) and creating two T-surfaces overlapping at intersection with priority fault (c), (d) after repairing.

for detecting and ranking faults and blocks (Baranov et al., 2004; Zakharova and Yampolsky, 2009).

5. Stability of ground within the Irkutsk urban territory

Faults and blocks have been detected and ranked in ArcMap 10 based on data obtained at the previous stage of work, following the principle that a block has the same rank as the bounding faults. In the resulting pattern, faults of five size grades cut the Irkutsk area into 99 blocks (Fig. 5). The blocks are of two main size groups, distinguished with a simple histogram: small and large ones, called microblocks (size classes B, C, D, and E) and megablocks (grade A). The class E is assigned to the smallest blocks (<0.5 km^2), and the other size classes are 0.6–5.5 km^2 (D), 5.6–15 km^2 (C), and 16–60 km^2 (B) respectively.

The largest blocks (A) bounded by the Angara and Irkut-Ushakovka fault systems are of special importance for the stability assessment (Lobatskaya and Kotlobaeva, 2001). There are four blocks of this class in the study area (Fig. 6): Novolenino in the northwest (A"N"), Topka in the northeast (A"T"), Levoberezhny in the southwest (A"L"), and Pravoberezhny in the southeast (A"P"). Each exceeds 60 km^2 and consists of smaller blocks of different size classes (B through E). Relatively large faults (ranks II and III) bound ten B blocks, which also enclose smaller blocks (most often C and fewer D or E blocks). The C group consists of 18 blocks having quadrangular (rhombic, trapezoidal, rectangular, etc.) or triangular geometries in map view, each comprising several D and E blocks. The blocks of grade D are the most abundant (56) and most diverse in geometry. Most of them are rectangular, quite many are isometric, and fewer are triangles. The smallest E blocks are rare (11 such blocks have been distinguished on the map scale); they appear at intersections of large faults and are triangles (more often) or quadrangles (Fig. 6).

To systematize faults and blocks, polygonal layers were created in the geodatabase, with such attributes as name, size (surface area), and deformation degree (function of fault density). The structures were classified using the equal interval method, with the number of classes estimated by Sturges's formula commonly applied in statistical calculations of this kind. Although looking

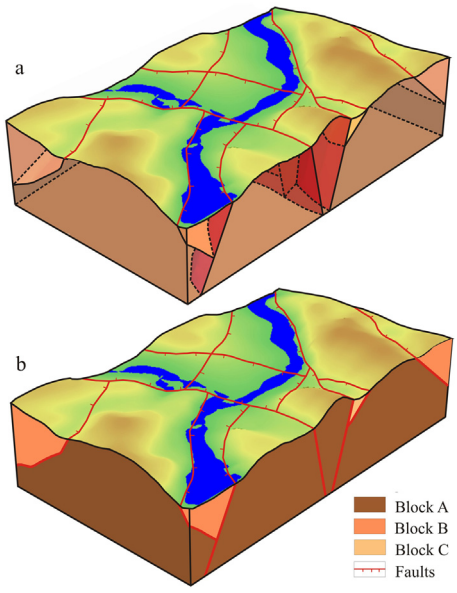

Figure 5. 3D solid model. (a) Initial version in translucent mode; (b) final version used for ground stability assessment.

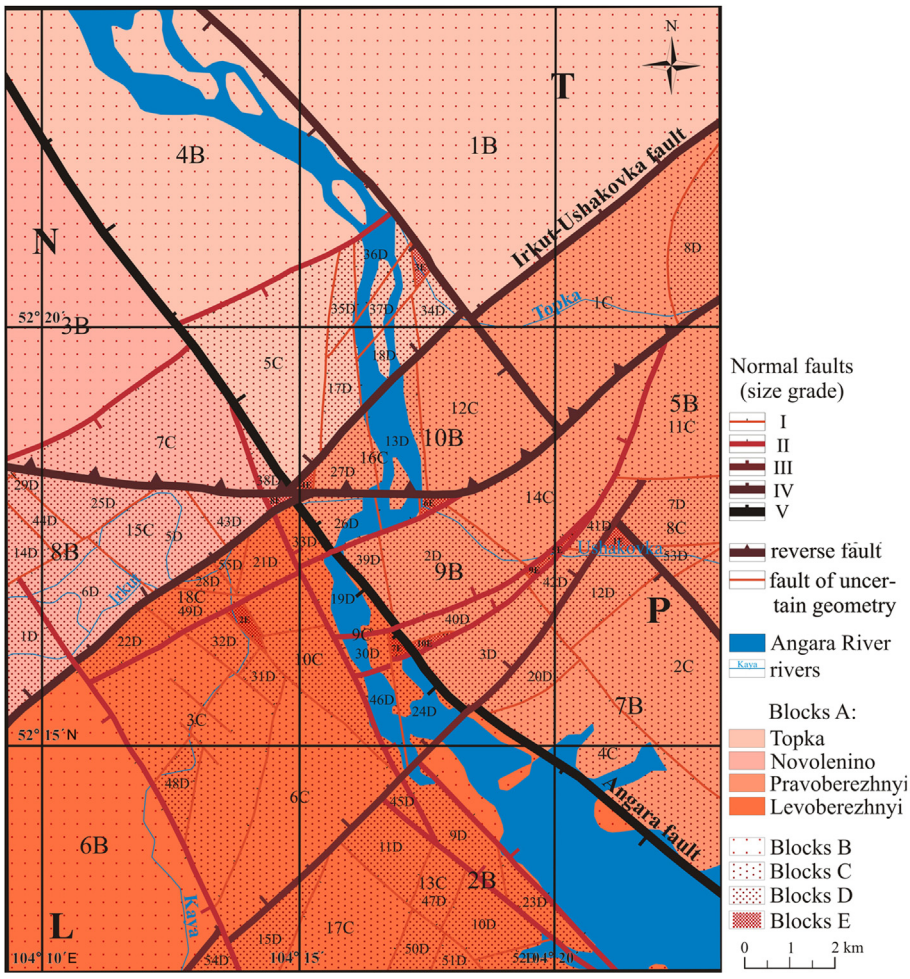

Figure 6. Map of faults and blocks.

chaotic in sizes and geometries, the classified blocks became organized in a well-knit system.

The geometry of blocks is another key parameter (besides the size) that records the deformation pattern in the crust and depends, on lithology and strength of rocks. The blocks of the Irkutsk territory are of diverse shapes due to the local sediment lithology (>1000 m thick Jurassic lagoonal-continental sandstone) and basement deformation, as large faults span both basement and sediments.

Each large block shows its own deformation pattern, with different numbers and strikes of faults inside the blocks and along block boundaries (crossing and bounding faults). Data were statistically processed using the conventional GIS options, which demonstrated their effectiveness in calculating the selected attributes from input data. The deformation degrees of blocks were estimated in arbitrary units per square kilometer using the attributes of rank and crossing/bounding position for faults and size class for blocks, selected when creating the geodatabase. The required parameters were calculated with the built-in ArcGIS calculator provided that the attribute values were specified in the attribute tables of the layers (Table 3).

The faults making block boundaries were rated on a five-grade scale according to their size ranks: grade 5 corresponded to rank V (>23.9 km), grade 4 to rank IV (18.2–23.8 km), grade 3 to rank III (12.5–18.1 km), grade 2 to rank II (6.8–12.4 km), and grade 1 was for the smallest faults of rank I (shorter than 6.7 km). In the rating of within-block faults, these values were duplicated (i.e., grades 10 to 2, correspondingly), taking into account the correlation between the fault length and the size of its damage zone (Table 3). The reasoning has been as follows: a fault boundary between two blocks always affects them both, while a crossing fault of the same rank deforms one and the same block; therefore, deformation is shared by two blocks in the former case and is all accommodated within one block, being thus twice bigger in the latter case.

The characteristics of faults and blocks are summarized in Table 3. Out of the four largest blocks, the Novolenino (Fig. 6, N) one appears to be the least deformed (about 0.3 a.u./km^2). It occupies more than 100 km^2 in the northwestern Anagara-Irkut interfluve and is bounded by the Irkut and Anagara faults in the south and northeast, respectively. There are two large faults that crosscut the block, striking at NW (330°) and NE (60°), respectively, and to 12 km long faults of ranks I and II are the most abundant. Novolenino, like three other largest blocks, is composed of plane-bedded thick Jurassic sandstones, with high water contents and other unfavorable engineering-geological properties.

The Topka block (Fig. 6, T), more than 77 km^2, is notably more strongly deformed (about 0.5 a.u./km^2) than the Novolenino one. The Angara and Irkut faults bound it in the southwest and south-southeast, respectively. The crossing faults strike mainly in the NE direction, at the azimuths from 40° to 65°, or at 10°, or sometimes to the northwest (at 320°).

Table 3
Characteristics of faults and blocks: a synthesis.

Block A	Number of smaller blocks (B,C,D,E) inside a Block A	S (km^2)	Faults, their ranks (r) and relation to blocks										Total fault rank (L)[a]	Fault density[b]	Ground stability (a.u./km^2) (Koff et al., 1996; Lobatskaya and Kotlobaeva, 2001)
			I		II		III		IV		V				
			Bd	Cr	Bd	Cr	Bd	Cr	Bd	Cr	Bd	Cr			
Levoberezhny	B = 2 C = 7 D = 26 E = 3	96	–	20	–	5	–	1	1	–	1	–	75	0.8	52–148
Novolenino	B = 2 C = 2 D = 10 E = 1	108	–	4	–	3	–	–	1	1	1	–	37	0.3	80–100
Pravoberezhny	B = 4 C = 8 D = 14 E = 6	94	–	8	–	4	–	1	1	2	1	–	63	0.7	58–101
Topka	B = 2 C = 1 D = 6 E = 1	77	–	7	–	1	–	–	1	1	1	–	35	0.5	99–110

Abbreviations stand for: S = block surface area; Bd = faults that bound blocks, Cr = fault that crosscut blocks.
[a] Total fault rank is found as $L = \sum_{Bd}(r \times n) + \sum_{Cr}(2 \times r \times n)$, where n is the number of faults.
[b] Fault density (ρ) is meant as number of faults per surface area, $\rho = L/S$ (a.u./km^2).

The Levoberezhny block (Fig. 6, L), occupying more than 96 km^2 in the Angara left bank, is located in the Irkut-Angara interfluve; the Irkut and Anagra faults delineate, respectively, its northern and northeastern boundaries. It is more heavily faulted than the two previous blocks (about 0.8 a.u./km^2), and is cut by faults striking mainly to the northwest at 315°–320° or to the northeast at 20°–60°.

The Pravoberezhny block (Fig. 6, R), 94 km^2, lies on the right bank of the Angara River, between the Irkut fault in the north and the Angara fault in the southwest. It is almost as deformed as the Levoberezhny block (about 0.7 a.u./km^2), and the orientations of faults in these two blocks are also similar: mostly NW (320°) and NE (40°, 60°), though some faults in the Pravoberezhny block strike roughly in the W–E direction. The faults of rank I are the most abundant in both blocks on the left and right river banks (Table 3).

Thus, the Levoberezhny and Pravoberezhny blocks in the southern part of the area are the most strongly deformed, the southeastern Topka block is deformed to a medium degree, and the Novolenino block in the northeast is the least deformed.

Earlier the natural stability of ground was estimated without man-caused loads in blocks of classes A, B, and C (Koff et al., 1996; Lobatskaya and Kotlobaeva, 2001). The blocks generally correspond to the historic administrative division of the city (Fig. 1), which followed the local geomorphic and tectonic features, such as watersheds, banks of the Angara River and its tributaries, valleys of small streams, etc. The ground stability was measured as a total score of expert points corresponding to destabilizing factors, i.e., the greater the score, the less stable the ground.

Thus estimated natural stability degrees vary in a broad range from very low (148 points) to very high (52 points). The highly stable blocks, coinciding with the Studgorodok (Polytechnical University) and Dekabristy Square neighborhoods (Fig. 1), are free from small faults and blocks of classes D and E. The blocks of medium stability, such as Akademgorodok and the localities of Rabochee and Marat, etc., often enclose local faults and small (D and E) blocks, but their stability is affected more by erosion, flooding, and loess soil subsidence than by fault density.

The blocks of low stability, in the swampy part of the Yubileinyi neighborhood and the part of the Topka neighborhood at the foot of a hill (Fig. 1), are split into numerous E blocks, while the destabilizing factors include primarily active and buried landslides induced by local faults.

Finally, the very low stability of the Ershov gulf block (Fig. 1) is mostly due to the regional Angara fault with its steep fault terrace where a buried landslide was reactivated by roadway excavation.

Therefore, heavily faulted blocks turn out to have even higher natural ground stability. This inference is not as paradoxical as it might seem if one takes into account the state of small blocks. The synthesis of data on the four largest A blocks in the Irkutsk area shows that the correlation between ground stability and deformation degree is not obvious (Table 3). For instance, the low deformation degree of 0.3 a.u./km^2 in the Novolenino block would mean a highly stable ground, but earlier estimates gave a total score of 80–100 expert points, which corresponds to a medium or low stability; or, the moderately deformed Topka block (0.5 a.u./km^2), has a low stability of 99–110 points. On the other hand, the stability of the youngest and most heavily deformed Pravoberezhny and Levoberezhny blocks of ~0.7 and 0.8 a.u./km^2, respectively, is very uneven: 58 to 101 and 52 to 148 points, respectively. The former range corresponds to rather high or medium stability, while the latter reflects different stabilities of the constituent blocks.

Thus, the pattern of faults and blocks obviously has to be considered in 3D, rather than in a map view, being aware that faults between blocks of different stability degrees are controlled by multiple factors.

6. Conclusions

GIS technologies open new avenues in studies of fault patterns due to fast processing of different datasets and easy data comparison on a single cartographic base. The GIS procedures, and specifically the ArcGIS tools, save a lot of time in mapping faults and blocks, as well as in analyzing the related 2D vector data. The options offered by ArcGIS were sufficient to create legends and fine tune the maps without using external software.

With mapping tools, the classes of spatial object were populated with vector and attribute information as a basis for digital mapping (Figs. 1 and 5). To avoid mapping errors in 2D modeling, the geometry of objects was checked against topology and corrected using the respective ArcGIS editing tools.

The faults were divided into five ranks according to lengths using the equal interval method of data classification, which made it possible to further classify faults and blocks with other methods. At the same time, the option of creating attribute tables, with a built-in calculator and geometry calculation, allowed estimating rapidly the fields of quantitative data. For reliable assessment of ground stability, 3D modeling was performed with regard to fault dips.

The reported GIS-based analysis of the fault pattern in the urban territory of Irkutsk city supports the idea of faulting control over ground stability but, on the other hand, it demonstrates that the deformation degree and stability of the ground are related in an intricate and ambiguous way.

In order to enhance the advantages of GIS in building and analyzing 3D models, predicting geological risks, and deriving other maps, the 3D model of the fault pattern has to be converted into the respective GIS format. At this stage of research, however, we have only visualized the near-surface in 3D. Although not being the final solution, this is a promising way to present 2D map data worth of further investigation.

References

ArcGIS Desktop, 2010. I. Version 2.1. 185 pp; II. Version 2.1., 364 pp; III. Version 2.1. 217 pp (in Russian).

Archegov, V.B., 2012. Crustal fault pattern and petroleum potential: theory and methods. Neftegazovaya Geologiya. Teoriya i Praktika (2). http://www.ngtp.ru/rub/8/22_2012.pdf (in Russian).

Baranov, Yu D., Busygin, B.S., Nikulin, S.L., 2004. 3D reservoir modeling for well placement. Gornyi Informacionno-Analiticheskii Byulleten 3, 197–201.

Bilibin, S.I., Dyakonova, T.F., Isakova, T.G., Istomin, S.B., Yukanova, E.A., 2007. Three-dimensional geological modeling as a critical step in reservoir studies. Nedropolzovanie XXI Vek 4, 38–42.

Breunig, M., Cremers, A.B., Götze, H.-J., Schmidt, S., Seidemann, R., Shumilov, S., Siehl, A., 1999. First steps towards an interoperable 3D GIS – an example from southern lower Saxony, Germany. Physics and Chemistry of the Earth, Part A 24 (3), 179–190.

Breunig, M., Cremers, A.B., Götze, H.-J., Schmidt, S., Seidemann, R., Shumilov, S., Siehl, A., 2000. Geological mapping based on 3D models using an interoperable GIS. Geo-information-systems. Journal for Spatial Information and Decision Making 13, 12–18.

Büttner, S.H., Sherlock, S., Fryer, L., Lodge, J., Diale, T., Kazondunge, R., Macey, P., 2013. Controls of host rock mineralogy and H_2O content on the nature of pseudotachylyte melts: evidence from Pan-African faulting in the foreland of the Gariep Belt, South Africa. Tectonophysics 608, 552–575.

Carlos, C.U., Francisco, H.R., Francisco, C.C., Rubson, P., Maria, O.L., 2014. Quaternary fault control on the coastal sedimentation and morphology of the San Francisco coastal plain, Brazil. Tectonophysics 633, 98–114.

Cassard, D., Billa, M., Lips, A.L.W., et al., 2004. An expert-guided data-driven approach and scale-related data models for multicriterion processing with GIS andes. In: GIS in Geology. International Conference, Moscow, 15–19 November, 2004. Vernadsky SGM RAS, Moscow, pp. 27–31. Extended Abstracts.

Cheremisina, E.N., Nikitin, A.A., 2006. Geoinformation systems for nature management. Geoinformatika 3, 5–20.

Gardoll, S., Groves, D., Knox-Robinson, C., et al., 2000. Developing the tools for geological shape analysis, with regional- to local-scale examples from the Kargoorlie Terrane of Western Australia. Australian Journal of Earth Sciences 5, 943–953.

Gonzalez, A., Vazquez-Prada, M., Gomez, J.B., Pacheco, A.F., 2006. A way to synchronize models with seismic faults for earthquake forecasting: insights from a simple stochastic model. Tectonophysics 424, 319–334.

Healy, D., Sibson, R.H., Shipton, Z.K., Butler, R.W.H., 2012. Stress, faulting, fracturing, and seismicity: the legacy of Ernest Masson Anderson. In: Healy, D., Butler, R.W.H., Shipton, Z.K., Sibson, R.H. (Eds.), Faulting, Fracturing and Igneous Intrusion in the Earth's Crust. Geological Society, London. Special Publication 367, pp. 1–6.

Koff, G.L., Lobatskaya, R.M., 1991. Fault Studies for Engineering-geological Surveys in Active Seismic Areas. PBG, Warsaw, p. 224.

Koff, G.L., Lobatskaya, R.M., Serova, G.U., 1996. Geological environment stability in earthquake prone urban areas. In: Natural Hazards, Land-use Planning and Environment. 6-th Spanish Congress and International Conference on Environmental Geology and Land-use Planning. Obra Completa, Spain, Granada, pp. 303–312.

Krasnoramenskaya, T.G., 2008. Correlation of Fault Patterns and Seismicity in the Altay-Sayan Area: a GIS Approach. Dissertation for Candidate Sci. Degree (Geology & Mineralogy). EC ROPR SO RAN, Irkutsk, p. 151 (in Russian).

Lobatskaya, R.M., 1987. Structural Zoning of Faults. Nauka, Moscow, p. 128 (in Russian).

Lobatskaya, R.M., 1997. Kinetic method of approach to assessment of geological environment stability under anthropogenesis loads. In: Engineering Geology and the Environment. Proc. International Symposium, Organized by the Greek National Group of IAEG, Athens, Greece, 23–27 June 1997. A.A. Balkema, Rotterdam-Brookfield.

Lobatskaya, R.M., 2001. Modelling the ground behaviour in urban areas. In: Engineering Geological Problems of Urban Areas. Proc. International Symposium. Ekaterinburg, Russia 30.07–02.08.2001. Akva-Press, Ekaterinburg, pp. 286–291.

Lobatskaya, R.M., 2008. Modelling the behaviour of ground under natural and man-caused loads. In: Advanced Information Technologies for Science. All-Russian Conference. Magadan 20–24 April 2008. SVNC DVO RAN, Magadan, pp. 205–208.

Lobatskaya, R.M., Koff, G.L., 1997. Lithospheric Faults and Emergency. REFIA, Moscow, p. 196 (in Russian).

Lobatskaya, R.M., Koff, G.L., 1998. Evaluation of geological environment stability in seismic urban areas. In: Eleventh European Conference on Earthquake Engineering, 6–11 September 1998, Paris, France. Abstract Volume. A.A. Balkema, Rotterdam-Brookfield, p. 479 (CD-ROM).

Lobatskaya, R.M., Kotlobaeva, T.A., 2001. Tectonic modeling of a city territory for ground stability assessment. In: Engineering Geological Problems of Urban Areas. Proc. International Symposium. Ekaterinburg, Russia 30.07–02.08.2001. Akva-Press, Ekaterinburg, pp. 275–286.

Lobatskaya, R.M., Krasnoramenskaya, T.G., 2010. GIS tools for correlation of tectonics and seismisity in the Altay-Sayan area, Russia. Geoscience Frontiers 1, 133–141.

Logatchev, N.A., 1991. Faulting in the Lithosphere. Zones of Extension. Nauka, Novosibirsk, p. 228 (in Russian).

Makarov, V.I., 2007. Evolutionary nature of structure formation in lithospheric material: universal principle for fractality of solids. Russian Geology and Geophysics 48 (7), 558–574.

Nengxiong, Xu, Tian, Hong, Kulatilake, Pinnaduwa H.S.W., Duan, Qingwei, 2011. Building a three dimensional sealed geological model to use in numerical stress analysis software: a case study for a dam site. Computers and Geotechnics 38, 1022–1030.

Paradigm Geophysical, 2007. GeoDepth. 3D Canvas – Solid Model Builder, p. 148.

Sankov, V.A., 1989. Penetration Depths of Faults. Nauka, Novosibirsk, p. 136.

Sherman, S.I., 1977. Physical Laws of Crustal Faulting. Nauka, Novosibirsk, p. 102.

Sherman, S.I., Lobatskaya, R.M., 1972. Correlation between earthquake origin depths and fault lengths in the Baikal rift zone. Doklady AN SSSR 205 (3), 581–583.

Sibson, R.H., 1987. Earthquake rupturing as a hydrothermal mineralizing agent. Geology 15, 704–707.

Sibson, R.H., 2001. Seismogenic framework for hydrothermal transport and ore deposition. Reviews in Economic Geology 14, 25–50.

Sibson, R.H., 2006. Au-quartz Mineralization near the Base of the Continental Seismogenic Zone. Geological Society, London. Special Publication 272, pp. 521–534.

Strelchenko, I.P., 2013. Building a 3D solid model for interpretation of reflection profiling data from the southern Siberian craton. In: Geosciences-2013. Geology for Exploration: Methods and Approaches. Proc. Techn. Conf. with International Participants. Aktualnye Problemy Izucheniya Nedr, Issue 13, pp. 266–270.

Thayer, M.R., Arrowsmith, J.R., Young, J.J., Fayon, A., Rymer, M.J., 2004. Geologic structure of middle mountain within the San Andreas fault zone near Parkfield, California. Eos, Transactions, American Geophysical Union 85 (47). Fall Meet. Suppl., Abstract T13A-1335. http://activetectonics.asu.edu/GIS/GIS.html.

Trufanova, N.V., Kazantseva, E.E., 2005. Depth-velocity modelling and its optimization for the conditions of southern Siberia. Tekhnologii Seismorazvedki 2, 37–41 (in Russian).

Trufanova, N.V., Naumova, Yu A., Ginzburg, I.V., Zaravnyaev, V.A., 2008. Optimisation of depth-velocity modelling and improving the quality of migration of VSP and well-log data. Tekhnologii Seismorazvedki 3, 29–34 (in Russian).

Zakharova, A.A., Yampolsky, V.Z., 2009. Digital 3D geological and fluid-dynamic modelling for advance in reservoir characterization. Problemy Informatiki 1, 48–52 (in Russian).